Thin-film composite hollow-fiber nanofiltration membranes prepared from benzonitrile containing disulfonated poly(arylene ether sulfone) random copolymers coated onto polyphenylene oxide…

Ohkame, Takashi ; Shibuya, Masafumi ; Nakagawa, Keizo ; Shintani, Takuji ; Matsuyama, Hideto ; Yoshioka, Tomohisa

(Citation)
Journal of Membrane Science,631:119336

(Issue Date)
2021-04-19

(Resource Type)
journal article

(Version)
Accepted Manuscript

Thin-film composite hollow-fiber nanofiltration membranes prepared from benzonitrile containing disulfonated poly(arylene ether sulfone) random copolymers coated onto polyphenylene oxide support membranes

Takashi Ohkame,[a, b *] Masafumi Shibuya,[a] Keizo Nakagawa,[b, c] Takuji Shintani,[b, c] Hideto Matsuyama,[c, d] and Tomohisa Yoshioka[b, c**]

[a] Research Center, Toyobo Co., Ltd., 1-1 Katata 2-Chome, Otsu, Shiga, 520-0292, Japan

[b] Graduate School of Science, Technology and Innovation, Kobe University, 1-1 Rokkodai, Nada, Kobe, 657-8501, Japan

[c] Research Center for Membrane and Film Technology, Kobe University, 1-1 Rokkodai, Nada, Kobe, 657-8501, Japan

[d] Department of Chemical Science and Engineering, Kobe University, 1-1 Rokkodai, Nada, Kobe, 657-8501, Japan

* Corresponding author: Takashi_Okame@toyobo.jp

** Corresponding author: tom@opal.kobe-u.ac.jp

Keywords: Polyphenylene oxide; Hollow-fiber membrane; Dip-coating; Sulfonated polymer; Nanofiltration membranes

Abstract

A new method for the preparation of chemically robust thin-film composite hollow-fiber (TFC-HF) nanofiltration membranes through a dip-coating process is reported. A negatively charged disulfonated poly(arylene ether sulfone) random copolymer (SPN-20) containing highly polar benzonitrile groups was utilized as a separation layer in a TFC-HF membrane. Only four polar aprotic solvents, N-methyl-2-pyrrolidone (NMP), dimethyl acetamide (DMAc), dimethyl formamide (DMF), and dimethyl sulfoxide (DMSO), proved to be good solvents for SPN-20 possibly due to its rigid chemical backbone and strong intermolecular interactions. In order to avoid dissolution or irreversible swelling of the polymeric supports in the dip-coating process, a polyphenylene oxide (PPO) hollow-fiber membrane was introduced as a novel substrate for TFC-HF fabrications. Solubility investigation using a framework of Hansen solubility parameters (HSPs) revealed that the PPO membrane is a suitable substrate for coating the SPN-20 copolymer due to its tolerance of polar aprotic solvents. By using DMSO as a coating solvent for the SPN-20 copolymer, TFC-HF membranes were successfully prepared with neither dissolution nor any damage to PPO supports. The dip-coating and drying processes were analyzed in detail to optimize the thickness and separation performance of TFC-HF membranes. The resultant membranes showed excellent rejection of Na_2SO_4 (> 98%) and an almost 100% rejection of negatively charged dyes along with a reasonable level of pure water flux (1.0 to 10.3 [$L \cdot m^{-2} \cdot h^{-1} \cdot bar^{-1}$]).

1. Introduction

Nanofiltration (NF) is categorized to be between reverse osmosis (RO) and ultrafiltration (UF) on the membrane filtration classification and is defined as the filtration by a membrane with pore size typically less than 2 nm [1]. The importance of NF technology is defined by the efficient removal of natural organic matter (NOM) [2,3], arsenic [4,5], pesticides [6], and charged dyes [7], and by energy cost that is much lower than that of RO. The transport mechanism of NF membranes has been intensively studied both theoretically and experimentally, and the rejection properties are known to depend not only on steric hindrance but also on the exclusion effects of Donnan electrical potential and Born energy [8,9]. The most successful polymeric NF materials have been crosslinked aliphatic and aromatic polyamides prepared by interfacial polymerization. Polyamide membranes have a weak amphoteric characteristic due to unreacted amino groups and carboxyl groups retained in a three-dimensional crosslinked polyamide network. The balance between the quantity ratio of amino groups and carboxyl groups plays an important role in membrane separation performance and anti-fouling properties [10–13]. Despite the superior permselectivity of polyamide membranes, the main drawback of polyamide-based thin-film composite (TFC) membranes is their susceptibility to chlorine [14].

As an alternative to polyamide membranes for water purification, sulfonated poly(arylene ether) copolymers have attracted both academic and industrial attention as they possess excellent oxidation resistance in addition to the capability of removing multi-valent ions and biological contaminants such as NOMs. A vast amount of research has pursued the development of ideal sulfonated poly(arylene ether) copolymers for NF, RO, and, more extensively for use in the research field of proton exchange membrane (PEM) fuel cells

[14,15,24,16–23]. The simplest method to obtain sulfonated copolymers is the post-sulfonation of commercially available engineering plastics such as polyphenylene oxide (PPO) [15,17], polysulfone (PSU) [18–20], polyethersulfone (PES) [21,22], and polyetheretherketone (PEEK) [23,24]. The drawback of the post-sulfonation technique, however, is the difficulty in controlling the degree of sulfonation (*DS*) and polymer chain scissions when strong sulfonation conditions are selected [16,22].

To improve reproducibility of the *DS* and increase both the dimensional stability and the charge density of the copolymers, researchers have developed di-sulfonated poly(arylene ether sulfone) copolymers via direct copolymerization using a 3,3'-disulfo-4,4'-dichlorodiphenylsulfone disodium salt (SDCDPS) monomer combined with various hydrophobic aromatic monomers [14,16]. Park et al. and Lee et al. have synthesized di-sulfonated poly(arylene ether sulfone) copolymers comprised of SDCDPS, 4,4'-dichlorodiphenylsulfone (DCDPS), and 4,4'-biphenol (the nomenclature of the copolymer is BPS-XX, where BPS is an acronym of Bi-Phenyl Sulfone and XX stands for the molar percentage of SDCDPS), and evaluated their desalination performance by fabricating TFC membranes using a brush coating [25,26]. On the other hand, Sakaguchi et al. improved the dimensional stability of SDCDPS-type copolymers by incorporating highly polar benzonitrile groups into hydrophobic segments [27]. Benzonitrile moieties enhance the intermolecular interactions of the copolymer so that the swelling of polymer matrices is suppressed and the adhesive force of the copolymer to the substrate is increased [28,29].

For the fabrication of TFC membranes, however, selection of the appropriate solvent for SDCDPS-type copolymers is not always a straightforward process. These copolymers show good solubility in polar aprotic solvents such as N-methyl-2-pyrrolidone (NMP), dimethyl

acetamide (DMAc), dimethyl formamide (DMF), and dimethyl sulfoxide (DMSO) with NMP being the most commonly used copolymerization medium [27,30]. Unfortunately, a commercial polymeric support such as polysulfone (PSU) cannot tolerate the polar aprotic solvents [31]. Other candidates that are used as common polymeric supports such as polyethersulfone (PES) [32–36] and polyvinylidene fluoride (PVDF) [37] also are soluble in these solvents. Therefore, one approach in the construction of TFC membranes is to find a coating solvent that can dissolve the SDCDPS-type copolymers without harming conventional polymeric supports. For instance, Lee et al. used concentrated formic acid as a coating solvent for the above-mentioned BPS-XX copolymers and successfully obtained TFC membranes for desalination [25]. Park et al. used benign solvents of BPS-XX copolymers instead of harsh formic acid and found that diethylene glycol could dissolve BPS-20 copolymers up to 7 wt% [26].

Another approach to obtain TFC membranes from a wide variety of sulfonated poly(arylene ether) copolymers is to establish a novel polymeric support membrane that could tolerate polar aprotic solvents. In the present study, we introduced a hollow-fiber membrane support derived from polyphenylene oxide (PPO) for such a purpose. PPO is an aromatic amorphous polymer with a high glass-transition temperature (T_g = 213 °C) and excellent hydrolytic and oxidative resistance [15]. PPO membranes and their derivatives have been studied mainly for use in gas separation [38–40] and pervaporation [41–43]. However, an application of PPO membranes as TFC supports in the water filtration industry has not been reported, possibly due to a solubility trend for PPO that differs from that of other common engineering plastics such as polysulfone.

In the present work, benzonitrile-containing disulfonated poly(arylene ether sulfone) copolymers (SPN-20) developed by Sakaguchi et al. [27] were examined for use as a separation layer for TFC membranes. SPN-20 copolymer has a solubility window that is narrower than that of BPS-type copolymers. As far as we could ascertain, viable solvents for use with SPN-20 are limited to only four choices: NMP, DMAc, DMF, and DMSO. We investigated the solubility of SPN-20 copolymers and PPO in a wide range of organic solvents using the concept of Hansen solubility parameters (HSPs), and we found that the PPO membrane was a suitable substrate for SPN-20 copolymers. Furthermore, we focused on preparing an outside-in type of thin-film composite hollow-fiber (TFC-HF) membrane comprised of PPO and SPN-20 copolymers via a dip-coating technique. We selected a hollow-fiber configuration because hollow-fiber membrane modules have a much larger surface area compared with other types of membrane modules [44,45]. Due to its superiority, the improved permeance of TFC-HF membranes should result in a more productive membrane module. To optimize the thickness of the TFC-HF membrane, the dip-coating and drying processes were analyzed in detail. The nanofiltration performances of the resultant TFC-HF membranes are noted herein.

2. Experimental

2.1. Materials

The PPO hollow-fiber membranes used as supports for the TFC-HF membranes in this study were acquired from Toyobo Research Center, Japan. The membranes were spun using a dry-jet wet spinning method (details of the spinning conditions are not shown here). A disulfonated monomer, 3,3’-disulfo-4,4’-dichlorodiphenylsulfone disodium salt (SDCDPS, 99% purity), was acquired from the Konishi Chemical Industry, Japan. The SDCDPS was dried

in a vacuum oven overnight at 150 °C before use. Other monomers, 4,4'-biphenol (BP, 99.9% purity, Honshu Chemical Industry, Japan) and 2,6-dichlorobenzonitrile (DCBN, 99.7% purity, Evonik Industries, Germany) were used as received. All other chemicals were of reagent grade and used without further purification.

2.2. Synthesis of a nitrile group containing disulfonated copolymer (SPN-20)

Disulfonated poly(arylene ether sulfone) random copolymers comprised of monomer units of the SDCDPS, DCBN, and BP (denoted as SPN-XX, where SPN is an acronym of Sulfonated, Polymer, and Nitrile and XX is the molar percentage of SDCDPS) were synthesized via direct polycondensation in NMP using potassium carbonate (K_2CO_3) as a catalyst. The Chemical structure of the SPN-XX copolymer appears in Fig. 1. Based on the results of ^{1}H-NMR measurement (Varian 400MHz), the copolymer used in this study (SPN-20) possesses a degree of sulfonation (*DS*) (18.8%), which corresponds to an ion exchange capacity (IEC_p) of 1.07 meq/g. The weight average and the number average molecular weights (M_w and M_n) of the SPN-20 copolymer were 126,000 and 54,600, as determined by gel permeation chromatography (GPC, Shodex GPC-101, columns: TSK gel GMH_{XL}×2 + $G2000H_{XL}$, TOSOH) that is based on polyethylene glycol (PEG) standards. DMAc with 30 mM lithium bromide was used as a solvent for GPC measurements. The dry polymer density and the water uptake of the SPN-20 copolymer ρ_p were evaluated by measuring the dimensions and weights of cast films and proved to be 1.31 ± 0.02 g/cm^3 and 5.5 ± 0.3%, respectively. Further details of the synthesis and characterization methods for SPN-20 copolymers are provided in the Supporting Information. The ^{1}H-NMR spectrum of SPN-20 appears in Fig. S1.

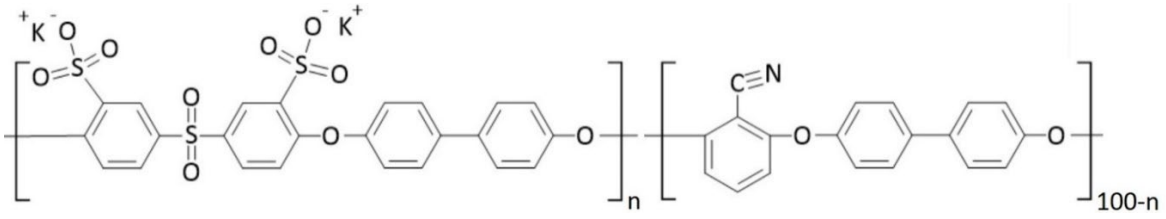

Fig. 1. Chemical structure of the sulfonated poly(arylene ether sulfone) copolymer (SPN-XX)

2.3. Characterization of PPO hollow-fiber membranes

The properties and scanning electron micrograph (SEM) images of PPO hollow-fiber membranes appear in Table 1 and in Figs. 2 and 3. The maximum pore diameter of the outer surface of the membrane proved to be ca. 30 nm.

Table 1: Properties of the PPO-HF membrane support.

Membrane material	Filtration mode	Outer diameter (μm)	Inner Diameter (μm)	Pure water permeance ($L \cdot m^{-2} \cdot h^{-1} \cdot bar^{-1}$)
PPO	Outside-in	268	150	91

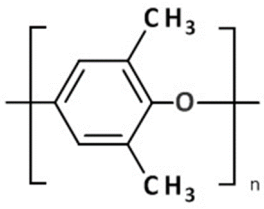

Fig. 2. Chemical structure of polyphenylene oxide (PPO)

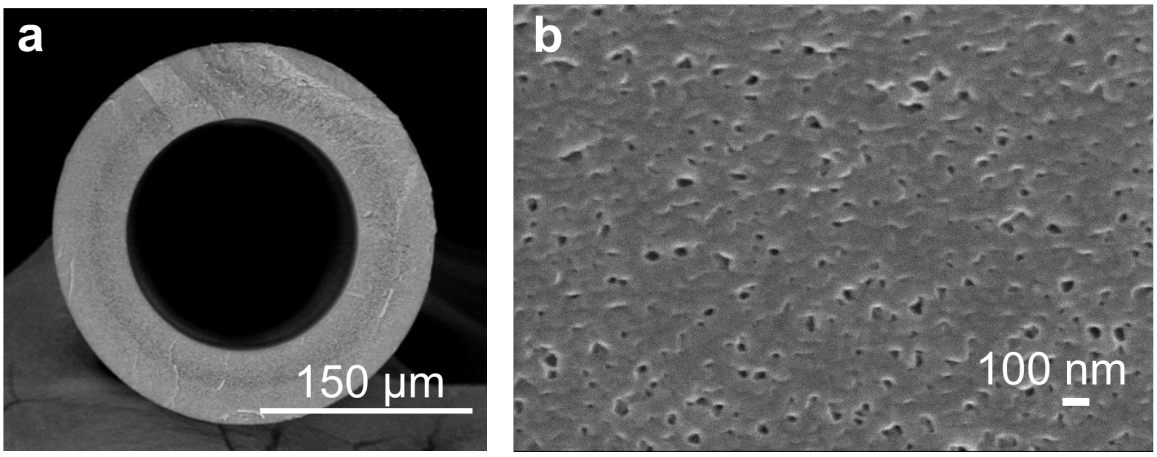

Fig. 3. SEM images of a PPO hollow-fiber membrane. (a) Cross-sectional view of a hollow-fiber membrane. (b) The porous structure of the outer surface.

2.4. Solubility tests of PPO polymers and SPN-20 copolymers and HSP evaluation

To investigate the PPO tolerance to polar aprotic solvents, 5 w% of PPO powder (181781, Sigma-Aldrich Japan) was dispersed in various polar aprotic solvents and heated to boiling temperature under refluxing with vigorous stirring for at least 1 hour. Common good solvents known to be viable for PPO are cited in the literature [15]. The solubilities of the SPN-20 copolymer were determined using 1 wt% solutions in a wide range of solvents after 24 hours with stirring at room temperature. Based on the obtained solubility data, the Hansen solubility parameters (HSPs) of PPO and SPN-20 were evaluated using the sphere technique that is a feature of HSPiP software [46]. With the HSP concept, the total (Hildebrand) solubility parameter, δ, is divided into the contributions from three types of intermolecular forces, as shown in Eq. (1).

$$\delta = \sqrt{\delta_{\mathrm{d}}^2 + \delta_{\mathrm{p}}^2 + \delta_{\mathrm{h}}^2} \quad (1)$$

In Eq. (1), δ_d is the dispersion term (Van der Waals force), δ_p is the polarity term (dipole-dipole interaction), and δ_h is the hydrogen-bonding term. Units are $(MPa)^{1/2}$. The distance between two substances (R_a) in the three-dimensional coordinate, (δ_d, δ_p, δ_h), is established by Eq. (2).

$$R_a = \sqrt{4(\delta_{d2} - \delta_{d1})^2 + \left(\delta_{p2} - \delta_{p1}\right)^2 + (\delta_{h2} - \delta_{h1})^2} \quad (2)$$

In Eq. (2), subscripts 1 and 2 represent each substance. The HSP values and the interaction radii (R_0) of PPO and SPN-20 were determined by computing valid spheres wherein good solvent groups inside a sphere ($R_a < R_0$) would be separate from non-solvent groups outside a sphere ($R_a > R_0$).

2.5. Fabrication of thin-film composite hollow-fiber (TFC-HF) membranes

TFC-HF membranes were fabricated using the dip-coating apparatus described in Fig. 4. An as-spun single PPO hollow-fiber membrane in a wet state was continuously supplied from an unwinder at a velocity of v = 3 m/min. A section of the hollow-fiber membrane was then immersed in a pretreatment bath containing 50 wt% glycerol aqueous solution heated at 60 °C for 30 seconds to fill the surface pores with viscous glycerol. Such pore-filling treatments using glycerol or glycol-type solvents [26,47] are important processes that suppress penetration into the pores of support membranes by the molecules of coating polymers and also suppress shrinkage of the support membrane pores from heat treatment during subsequent drying steps. Excess glycerol solution that had adhered to the fiber surface was then rubbed off by passage through several driving rollers. The fiber then was dipped in a coating bath filled with a dilute SPN-20 copolymer solution in DMSO at room temperature for ca. 2 seconds. The fiber was then drawn up vertically from the bath and guided into a forced convection oven. The height of the convection oven was 220 cm and the drying time was 44 s. In the drying step, it is

important to precisely control the temperature and velocity of the air flow inside the oven to ensure reproducibility of the TFC-HF membrane performance. Heated air was introduced vertically from the bottom of the oven and drawn from the top with the assistance of an exhaust fan. By controlling the balance of this push-pull type of airflow, the average flow velocity was maintained at 1.1 m/s (at standard temperature and pressure, STP) in order to minimize the fiber oscillation from turbulence. The static pressure in the oven was kept constant at slightly lower than atmospheric pressure (Δp = -2 to -2.5 Pa) to avoid a leakage of hot air from the fiber inlet and outlet. The temperature of the hot air along the entire fiber path in the oven was monitored and kept constant using a hot air generator and three independent heating plates attached to the wall of the oven. The tension of the fiber as it ran between the driving rollers and the winders was adjusted to less than 0.06 N, which was sufficiently below its yield force (typically 0.3 N). After drying, the resultant TFC-HF membrane was wound onto a large wheel-like spool to obtain a straight fiber bundle.

A schematic representation of the vertical dip-coating appears in Fig. 5. The basic relationship of liquid film entrained by a fiber being withdrawn from a coating bath can be written as Eq. (3), according to White and Tallmadge [48,49].

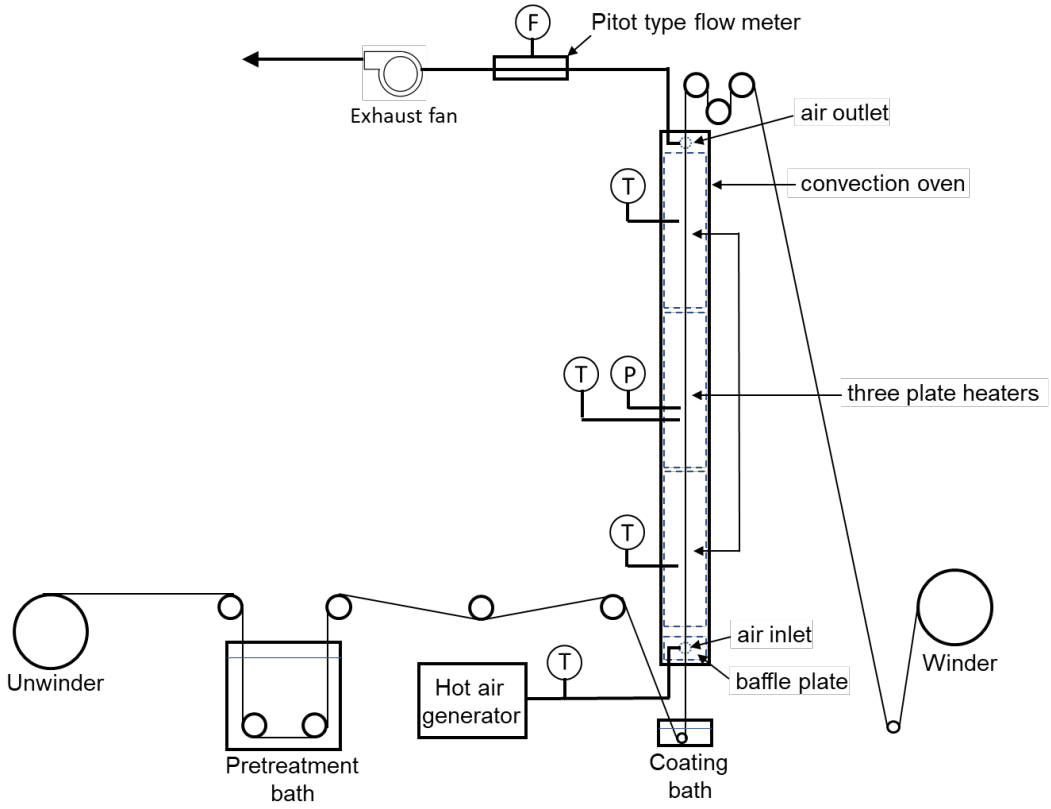

Fig. 4. Dip-coating and drying system for fabricating TFC-HF membranes. Symbols T, P, and F represent thermometers, pressure indicators, and flow meters, respectively.

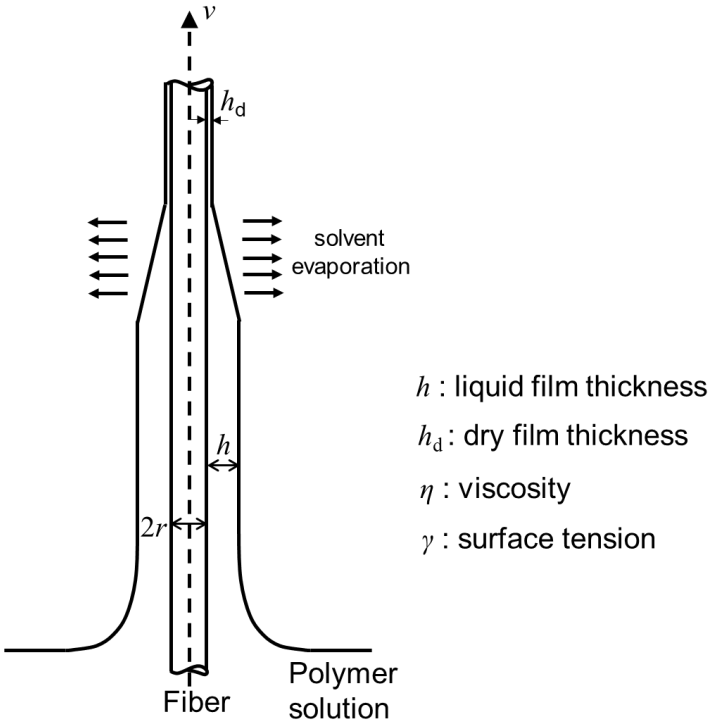

Fig. 5. Schematic representation of a vertical dip-coating process.

$$h = \frac{1.34 r Ca^{\frac{2}{3}}}{1 - 1.34 Ca^{\frac{2}{3}}} \quad (3)$$

In Eq. (3), h is the liquid film thickness, r is the fiber radius, and Ca is the capillary number, which is defined by Eq. (4).

$$Ca = \frac{\eta v}{\gamma} \quad (4)$$

In Eq. (4), η and γ are the viscosity and surface tension of a coating solution. v is the fiber speed. Eq. (3) is a corrected form of the original Landau-Levich-Derjaguin (LLD) equation, $h = 1.34 r Ca^{2/3}$, where the ratio of the liquid film thickness to the fiber radius, h/r, is no longer negligible [49]. In the present study, the coating velocity was kept constant (v = 3.0 m/min) and the surface tension was assumed to be equal to the value of pure DMSO (γ = 42.9 mN/m). Therefore, the solution viscosity, η, is the only variable of Ca. The viscosity of SPN-20

solutions was controlled by varying the polymer concentration, C_p. The relationship between η and C_p was derived from zero shear viscosity measurements (Physica MCR302 rheometer, Anton-Paar GmbH, Austria) using a 50 mm cone-plate geometry with a truncation of 1° (the viscosity data are shown in Fig. S2. Please refer to the Supporting Information). A polynomial fit to the viscosity data was used as follows: $\eta = 0.8049\ C_p^{\ 3} - 1.6742\ C_p^{\ 2} + 7.1916\ C_p + 1.6735$.

2.6. Characterization of TFC-HF membranes

2.6.1. Membrane surface roughness by AFM

The topographies of the outer surface of TFC-HF membranes were measured in the dynamic force mode (tapping mode) of atomic force microscopy (AFM, E-sweep/SPI4000 system, SII Nanotechnology Inc., Japan). A surface area of 2.0 μm × 2.0 μm was scanned using a 20 μm-scanner and Si-DF20 cantilevers. The average surface roughness ($R_{AFM,}$ instead of R_a which was already used for equation (2)) was calculated from each scan profile.

2.6.2. Elemental composition of a membrane surface via XPS

The elemental compositions of the surfaces of TFC-HF membranes were analyzed by X-ray photoelectron spectroscopy (XPS, K-Alpha$^+$ system, Thermo Fisher Scientific Inc., USA) using an X-ray with a beam spot size of ca. 200 μm generated from a monochromatic Al-Kα source operated at 12 kV and 2.5 mA. A wide first scan within a binding energy range of from 0 to 1,350 eV was recorded using a pass energy of 200 eV with 1 eV per step. Subsequent narrow scans to analyze the composition ratio of each element were recorded with pass energies of 50 eV at 0.1 eV per step.

2.6.3. Separation layer thickness

The thicknesses of the separation layers of TFC-HF membranes were evaluated via two independent methods.

(I) Fiber titration method: The ion exchange capacity of TFC-HF membranes (IEC_f) was measured via the titration of fiber samples. A 50 m length of a TFC-HF membrane was cut into small pieces that were then dispersed into 100 mL of a 2 M hydrochloric acid (HCl) solution under magnetic stirring for 24 hours. The fiber sample was then filtered and thoroughly rinsed with distilled water. Subsequently, the sample was dried in a vacuum oven at 150 °C overnight to remove the residual water and HCl. The dried fiber sample was weighed and dispersed in 1 M sodium chloride solution under stirring to release all the protons. After the pH stabilized, the amount of detached free protons was measured using 0.1 M sodium hydroxide solution in an automatic titrator (COM-1700, Hiranuma Sangyo, Japan). The average thickness of the separation layer (h_d) was calculated numerically via Eq. (5).

$$IEC_f = \frac{m_{H^+}}{W_d} = \frac{m_{H^+}}{\pi\{(h_d+r_f)^2-r_f^2\}\rho_p L} = IEC_p \quad (5)$$

In Eq. (5), m_{H^+} is the molar amount of protons exchanged via the titration and W_d is the dry weight of a charged polymer under investigation [50]. r_f is the fiber radius of the TFC-HF membrane after the drying process (r_f = 250 μm). ρ_p is the dry density of the SPN-20 copolymer (ρ_p = 1.31 g/cm^3). L is the fiber sample length (L = 50 m). Assuming that the density of the separation layer is equal to ρ_p, IEC_f should be equal to IEC_p (IEC_p = 1.07 meq./g) and thus h_d can be derived.

(II) TEM observation: The thickness of the actual coating layer of TFC-HF membranes was measured by transmission electron microscopy (TEM, JEOL JEM-2100, Japan). Membrane samples were embedded in an epoxy resin and an ultrathin section was prepared

using an ultramicrotome equipped with a diamond knife. A carbon-sputtered cross-section of the sample was observed at an accelerating voltage of 200 kV. At least five replicates were taken for each sample and the average thickness of the separation layer was measured.

2.7. Nanofiltration performances of TFC-HF membranes

A bundle of TFC-HF membranes was inserted into a plastic pipe and both ends of the fiber bundle were potted with a two-component epoxy resin. One side of the fibers embedded in the epoxy resin was cut with a knife to open a permeate exit. The number of fibers in a housing was typically 1,000 with a length of 30 cm. Before evaluation of the TFC-HF membranes, the fibers in a module were immersed in ethanol for 30 min to wet all the membrane pores, and the ethanol was gradually substituted by distilled water using a diaphragm metering pump. When the substitution was complete, the performance of the TFC-HF membrane modules was evaluated at 5 bar and 25 °C using a laboratory-scale crossflow filtration system. The concentrations of feed solutions were set at 1,500 mg/L and 200 mg/L for salt rejection tests and neutral solute rejection tests, respectively. For salt rejection tests, a conductivity meter (DS-72, HORIBA, Japan) was used to measure the salt concentration of the feed and permeate solutions. For neutral solute rejection tests, the concentrations of carbohydrates were determined by the phenol-sulfuric acid method described by Dubois [51]. The absorbance was measured at 490 nm using a UV-vis spectrophotometer (UV-2450, SHIMADZU, Japan). For removal tests of organic dyes, Sunset Yellow (Mw= 452.36) and Evans Blue (Mw = 960.79) were examined at concentrations of 100 mg/L. The concentration of each dye was estimated by interpolation to predetermined calibration curves at light wavelengths of 482 nm for Sunset Yellow and 606 nm for Evans Blue using a UV-vis

spectrophotometer. The observed rejection, R_{ej}, and the water permeate flux, $J_{w,}$ were calculated using Eqs. (6) and (7), respectively.

$$R_{ej} = \frac{c_f - c_p}{c_f} \times 100 \quad (6)$$

In Eq. (6) c_f and c_p are the feed and permeate concentration, respectively.

$$J_w = \frac{\Delta V}{A_m \cdot \Delta t} \quad (7)$$

In Eq. (7), ΔV is the permeate volume collected during a time period, Δt. A_m is the outer surface area of the TFC-HF membrane. Pure water permeance, L_p, was evaluated according to Eq. (8) using distilled water as the feed.

$$L_p = \frac{J_w}{\Delta P} \quad (8)$$

The molecular weight cut-off values (MWCO, at R_{ej} = 90%.) of TFC-HF membranes were evaluated by fitting the rejection data for neutral solutes (glucose, sucrose, raffinose, α-cyclodextrin, and γ-cyclodextrin) using the horizontal asymptote [52] with Eq. (9).

$$R_{ej} = \frac{1}{(1+M_w/B)^C} \quad (9)$$

In Eq. (9), M_w is the molecular weight, and B and C are fitting parameters.

3. Results and Discussion

3.1 . Hansen Solubility parameters of PPO and SPN-20 copolymer

Instead of a three-dimensional HSP diagram, it is more convenient to use a triangular diagram in order to visually comprehend the positional relationships of polymers and solvents [26,53,54]. The contribution of each component, F_i, to the total solubility parameter is written as Eq. (10).

$$F_i = 100 \times \left(\frac{\delta_i}{\delta_d+\delta_p+\delta_h}\right) \quad (10)$$

Figs. 6a and 6b show the solubilities of PPO and SPN-20 in various solvents. All solubility data were experimentally determined with the exception of that for the good solvents for PPO, which were cited from the literature [15]. From the Hansen sphere method, The HSP values were determined as δ_d = 17.3, δ_p = 4.6, δ_h = 2.7 for PPO and δ_d = 17.6, δ_p = 14.0, δ_h = 9.5 for SPN-20. For details of the fitting results in the three-dimensional Hansen sphere, please refer to Fig. S3 in the Supporting Information.

PPO is basically soluble in low polar solvents such as halogenated solvents and aromatic hydrocarbons, as shown in Fig. 6a. The use of these solvents, however, is not recommended for a membrane fabrication process due to their high toxicity and carcinogenicity. On the other hand, we discovered that under an elevated temperature PPO was soluble in four polar aprotic solvents: N-methyl-2-pyrrolidone (NMP), dimethyl acetamide (DMAc), tetrahydrofuran (THF), and dimethyl formamide (DMF). These solvents are referred to as 'poor' solvents, because they have a certain theta temperature at which a polymer-polymer attraction force exceeds the polymer-solvent attraction force. Other polar aprotic solvents such as dimethyl sulfoxide (DMSO), γ-butyrolactone (GBL), and sulfolane were non-solvents in this instance, and PPOs were completely insoluble even when their boiling temperatures were approached.

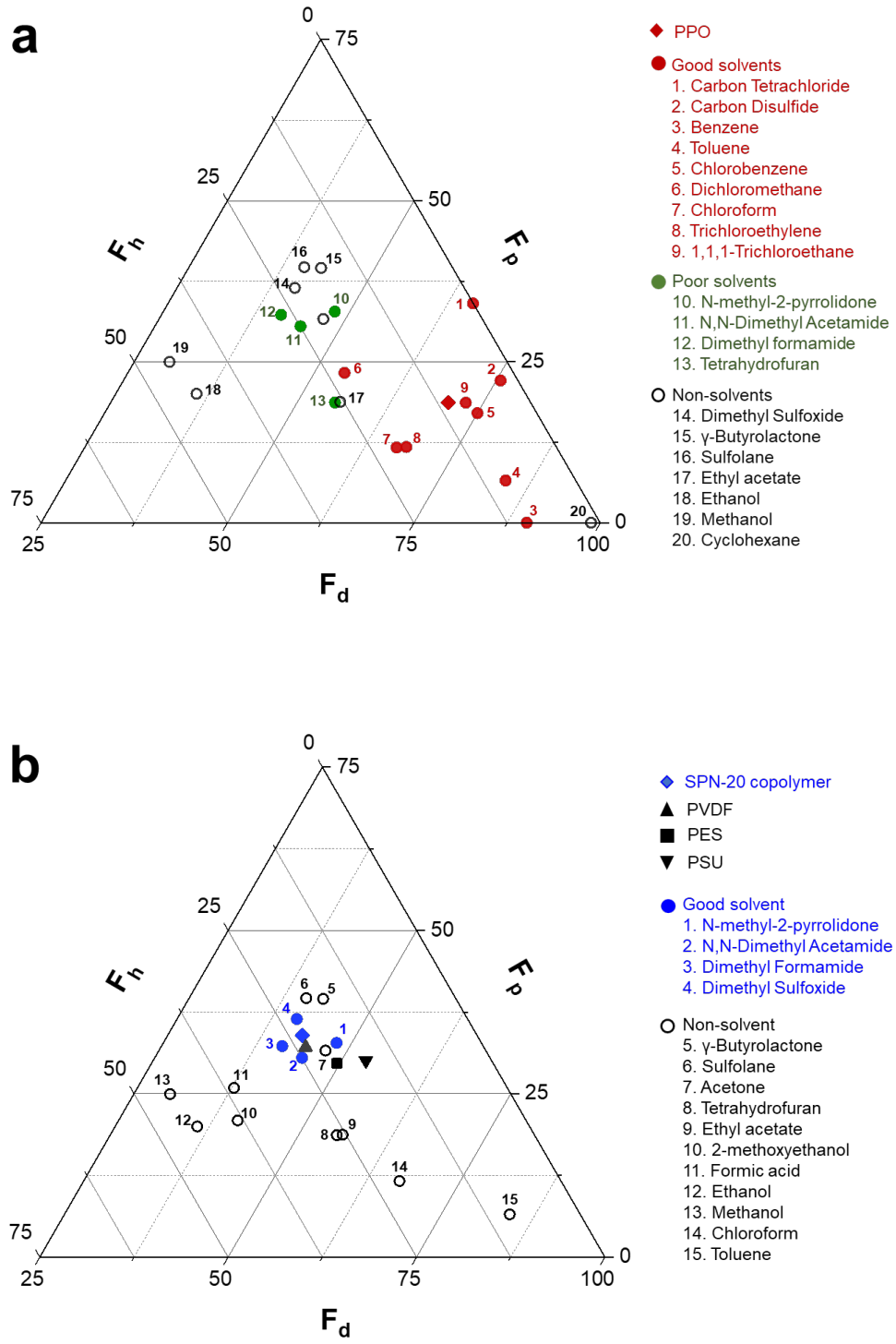

1

2

3

4 Fig. 6. Triangular diagrams of Hansen's solubility parameters. (a) PPO and (b) SPN-20

5 copolymer.

6

Fig. 6b shows that the solubility window of the SPN-20 copolymer was quite narrow. Only four polar aprotic solvents (NMP, DMAc, DMF, and DMSO) were found to be good solvents. Formic acid [25] and 2-methoxyethanol [47] were used to coat other sulfonated poly(arylene ether) copolymers, but were non-solvents for SPN-20, possibly due to strong intermolecular forces between the benzonitrile groups in their hydrophobic segments. Similarities were established among the HSPs of other common polymers utilized for ultrafiltration membrane supports with SPN-20 copolymer: PVDF (δ_d = 17.2, δ_p = 12.5, δ_h = 9.2) [46,55]; PES (δ_d = 18.8, δ_p = 11.3, δ_h = 7.9) [56]; and, PSU (δ_d = 19.8, δ_p = 11.2, δ_h = 6.2) [46,57]. Also, their distances, R_a, from the SPN-20 copolymer were R_a = 1.74, 3.96, 6.11, respectively. Indeed, these polymers were found to be either soluble or intensely swollen in NMP, DMAc, DMF, and DMSO, which rendered them inappropriate as a support membrane.

As a result of the above-mentioned observations, DMSO proved to be the most appropriate coating solvent that could form a homogeneous, stable SPN-20 coating solution that would not harm PPO support membranes. It is also important that DMSO is a low toxicity solvent (LD_{50} = 14,500 mg/kg for rat) and has a relatively low vapor pressure (B.P. = 189 °C), which enables a stable dip-coating process that maintains the solution surface in a coating bath to prevent unfavorable skin formation via rapid evaporation.

3.2 . Analysis of the separation layer thicknesses of TFC-HF membranes

Optimizing the thickness of the separation layer of TFC-HF membranes is a crucial issue. As equations (3) and (4) show, liquid film thickness, *h,* can be calculated theoretically. Subsequently, the average thickness of the dry film, h_d, was computed using Eqs. (11) and (12).

$$S_d = \Phi_p S_w = \Phi_p \pi\{(h + r_i)^2 - {r_i}^2\} = \pi\{(h_d + r_f)^2 - {r_f}^2\} \quad (11)$$

$$\Phi_{\mathrm{p}} = \frac{C_{\mathrm{p}}/\rho_{\mathrm{p}}}{\{C_{\mathrm{p}}/\rho_{\mathrm{p}}+(1-C_{\mathrm{p}})/\rho_{\mathrm{s}}\}} \quad (12)$$

In Eqs. (11) and (12), S_{d} and S_{w} are the average cross-sectional areas of the dry and liquid films, respectively. φ_{p} is the volume fraction of the SPN-20 copolymer based on a simple mixing rule. r_{i} and r_{f} are the fiber radii before and after the drying process (r_{i} = 268 μm and r_{f} = 250 μm). ρ_{s} and ρ_{p} are the densities of DMSO at 25 °C and a SPN-20 copolymer (ρ_{s} = 1.1 g/cm^3 and ρ_{p} = 1.31 g/cm^3), respectively. From these equations, h_{d} was numerically determined.

Fig. 7 compares the thicknesses estimated by two experimental methods (fiber titrations and TEM observations) and displays the theoretical calculations. Fig. 8 features TEM images of the TFC-HF membranes. The h_{d} values, as estimated using the theory by White and Tallmadge (solid line), for fiber titration (open circle) and TEM observation (open triangle), were in very good accordance at C_{p} = 0.75 and 1.5 wt%. However, at high C_{p} > 2.0 wt%, experimental measurements showed that two thicknesses started to greatly exceed the theoretical values. The possible reason for this deviation could be attributed to a coagulation effect that was not considered in the theory. In the dip-coating process (Fig. 4), a hollow-fiber was impregnated with glycerol aqueous solution as a pretreatment. When a fiber made contact with the SPN-20/DMSO solution, an increase in viscosity due to the aggregation of SPN-20 copolymers would occur at the fiber interface, which then led to an increase in the actual capillary number C_{a}. The coating thickness became unstable at $C_{\mathrm{p}} \geq$ 3.0 wt% and a 'pearl-string' type of structure [49] was visually observed when a fiber was withdrawn from the coating bath. Therefore, the thickness measurement by TEM could not be performed correctly at $C_{\mathrm{p}} \geq$ 3.0 wt%.

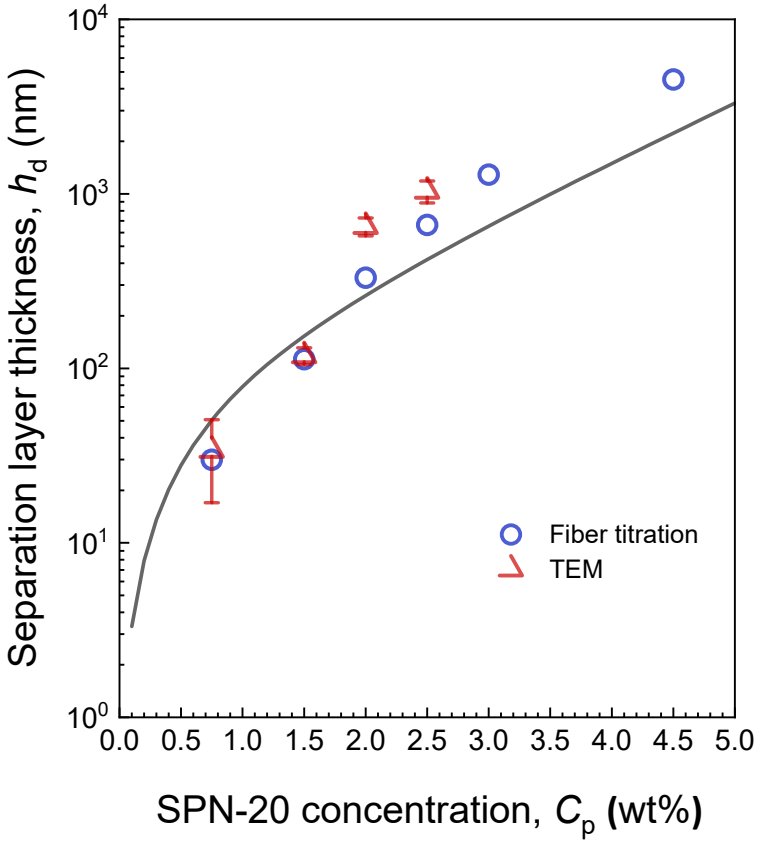

1

2 Fig. 7. Comparison of coating layer thicknesses as measured by two experimental methods.

3 The solid line represents the theoretically derived thickness from equations (3), (4), (11), (12).

4

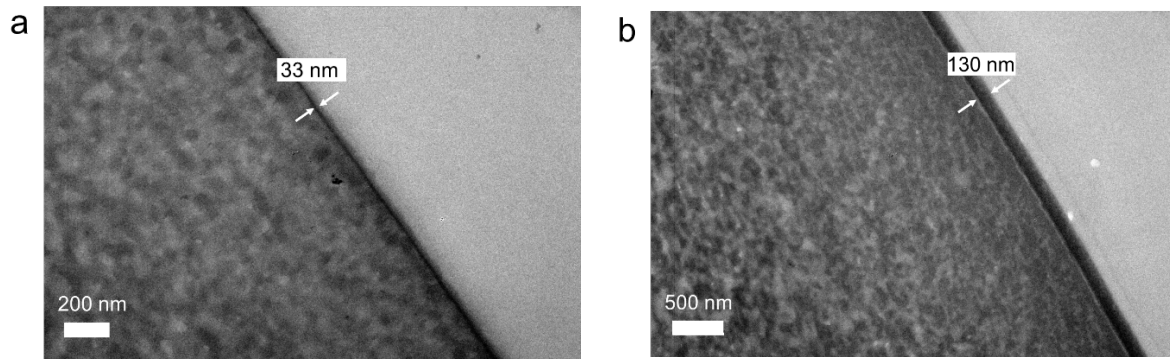

5

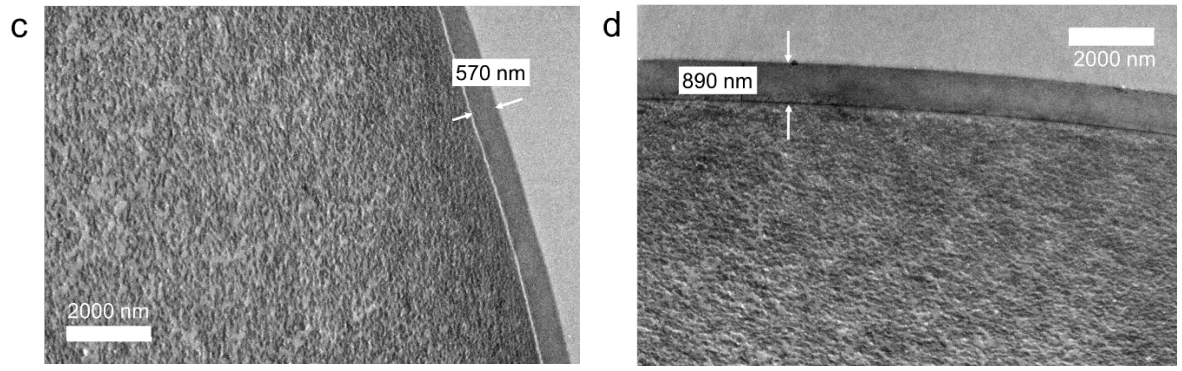

Fig. 8. Comparison of coating layer thicknesses, as measured via TEM. (a) C_p = 0.75 wt%, (b) C_p = 1.5 wt%, (c) C_p = 2.0 wt%, and (d) C_p = 2.5 wt%.

3.3 . Elemental compositions and morphologies of TFC-HF membrane surfaces

The elemental compositions and morphologies of the surfaces of PPO support membranes and TFC-HF membranes were analyzed via XPS (Table. 2) and AFM (Fig. 9) measurements. The elemental composition of the outer surface of the PPO hollow-fiber membrane was consistent with the calculation value for PPO. Regarding the surface of TFC-HF membranes prepared under dip-coating conditions of C_p = 0.75 to 3.0 wt%, the elemental compositions were also consistent with the calculated value of SPN-20, and the increases in sulfur and nitrogen elements were attributed to sulfonic and nitrile groups in the SPN-20 chemical structure. Based on the AFM measurements shown in Fig. 9, the surface roughness was drastically decreased after dip-coating due to the formation of a smooth separation layer of the SPN-20 copolymer. However, large standard deviations of R_{AFM} were observed for C_p = 0.75 wt% (R_{AFM} = 1.87 ± 0.50 nm), which indicated that the formation of the separation layer was incomplete. These results correspond with a large error in the average thickness of the separation layer, as measured by TEM (34 ± 17 nm) at C_p = 0.75 wt%, as shown in Fig. 7.

Table 2: XPS elemental analysis of the surfaces of PPO support and TFC-HF membranes

	C (%)	O (%)	S (%)	N (%)	K (%)
PPO support	85.3 (± 0.44)	13.5 (± 0.40)	0.2 (± 0.03)	0.8 (± 0.21)	< 0.1
C_p = 0.75 wt%	78.3 (± 0.17)	15.3 (± 0.20)	2.3 (± 0.18)	3.7 (± 0.15)	0.2 (± 0.16)
C_p = 1.5 wt%	78.2 (± 0.54)	15.1 (± 0.29)	2.4 (± 0.05)	3.2 (± 0.36)	0.7 (± 0.09)
C_p = 3.0 wt%	77.7 (± 0.39)	14.8 (± 0.17)	2.6 (± 0.03)	3.4 (± 0.29)	1.2 (± 0.04)
PPO (Calculation)	88.9	11.1	-	-	-
SPN-20 (Calculation)	79.2	13.9	2.2	3.2	1.49

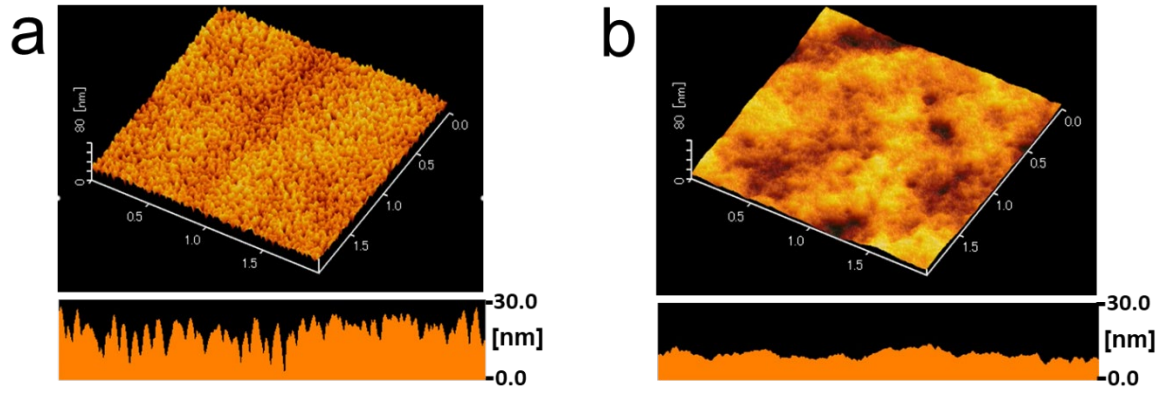

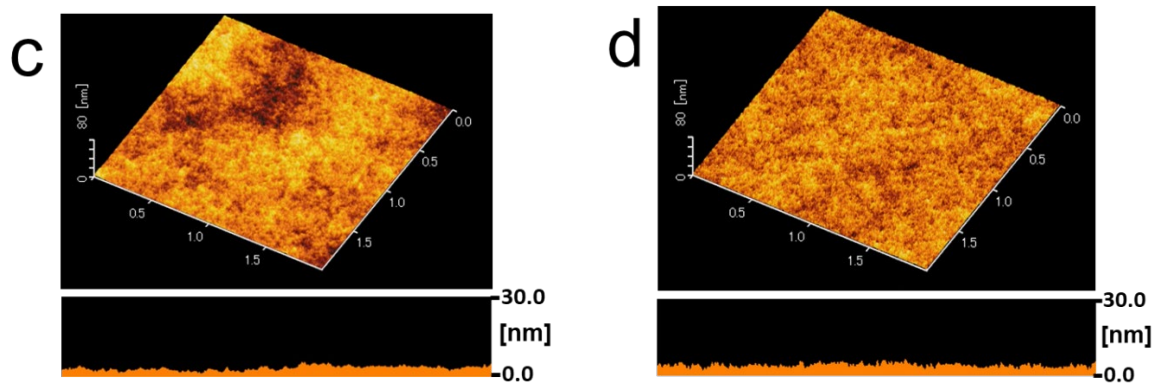

Fig. 9. Comparison of the membrane surface roughness of TFC-HF membranes via AFM. (a) PPO hollow-fiber support: R_{AFM} = 3.30 ± 0.24 nm, (b) TFC-HF: C_p = 0.75 wt%, R_{AFM} = 1.87 ± 0.50 nm, (c) TFC-HF: C_p = 1.5 wt%, R_{AFM} = 0.69 ± 0.03 nm, and (d) TFC-HF: C_p = 3.0 wt%, R_{AFM} = 0.77 ± 0.02 nm.

3.4 . Effect of drying conditions on TFC-HF membrane performances

In addition to the coating thickness control, the drying condition is another important factor that determines TFC-HF membrane performance. Here, we focused on the influence that drying temperature has on TFC-HF membrane performances at C_p = 1.5 wt%, for which the thinnest and defect-free separation layer could be obtained (an average thickness of 118 ± 13 nm via TEM observation). As for the dip-coating condition at C_p = 0.75 wt%, reproducible membrane performances could not be obtained.

Fig. 10 shows the glycerol content dependency on drying temperature retained in fiber samples after the dip-coating and drying processes, which is an indicator of both the extent of drying and the tightness of the separation layer. The glycerol content steeply declined from T_d = 165 to 170 °C and decreased gradually above 175 °C, which may correspond to a constant rate period and a decreasing rate period of drying. Figs. 11 and 12 show the MWCO and

rejection dependencies on drying temperature, respectively. At T_d = 165 °C, the SPN-20 separation layer was quite loose and the MWCO could not be determined within a molecular weight range of typical NF membranes (i.e., 200 to 2,000). In the present dip-coating system, the glycerol aqueous solution contained in PPO hollow-fiber supports plays the role of a coagulation agent for the SPN-20/DMSO liquid layer. Therefore, the competition between the drying rate of solvents from the surface of the liquid layer and the coagulation rate from inside the liquid layer would determine the final membrane structure. From T_d = 170 °C to 180 °C, the MWCO values decreased from 890 to 420, which indicated a smaller pore size of the separation layers as a result of drying which occurred much faster than coagulation could take effect.

One may consider these pore-tightening effects observed for TFC-HF membranes through high-temperature treatments might be caused by not only drying and coagulation but also chemical reactions (e.g. thermal cross-linking). However, the SPN-20 copolymer used in this study is thermally very stable and has a high glass transition temperature (T_g = 276 °C), which is close to the reported value for BPS-20 copolymer whose chemical structure is similar [58]. The thermal stability of SPN-20 was also confirmed by the fact that a SPN-20 film prepared on a glass plate heated at 180 °C readily dissolved in DMSO and no precipitate was observed. Regarding a PPO hollow-fiber support, the pure water flux after the same coating and drying treatment at 180 °C using pure DMSO in a coating bath instead of SPN-20/DMSO solution was 85 ($L \cdot m^{-2} \cdot h^{-1} \cdot bar^{-1}$) which is only slightly lower than that of the virgin PPO support (91 [$L \cdot m^{-2} \cdot h^{-1} \cdot bar^{-1}$]). PPO hollow-fiber supports showed no contribution to nanofiltration rejection performances. Thus, the pore structure of TFC-HF membranes in this study is indeed

determined by the balance between drying rate and coagulation rate of the SPN-20/DMSO liquid layer.

When drying temperature was set at below 160 °C, a fiber left from the oven was apparently very wet and the membrane performance was not reproducible, which indicates the insufficient drying led to the formation of a very weak gel layer. Therefore, the drying temperature range between 165 °C to 180 °C is favorable for obtaining a typical pore size of NF membranes. It should be noted that lowering local humidity in the oven is the crucial issue to determine the drying rate since the drying rate depends on a vapor pressure differential between a fiber surface and the air in the oven. Therefore, both the drying temperature and the air flow volume must be optimized. In this study, the flow velocity was preliminary determined to be 1.1 m/s (which corresponds to the air flow volume of 0.165 m^3/s at STP) due to the limitation that the fiber oscillation caused by turbulence must be minimized. Under the condition of this flow velocity, the optimum temperature range was empirically determined. However, an analysis of the relationship between a humidity of the mixed solvent and an air flow velocity in the oven would be quite complicated and beyond the scope of the present study.

The rejection data of several salts in Fig. 12 shows that the rejection values of Na_2SO_4 are excellent (R_{ej} = 82.5, 91.5, 99.2, 99.5% corresponding to T_d = 165, 170, 175, 180 °C). The rejection decreased on the order of Na_2SO_4 (mono-divalent) > NaCl ≈ $MgSO_4$ (mono-mono or di-divalent) > $CaCl_2$ (di-monovalent). The higher rejection of the mono-divalent type of salt compared with other types of salts was attributed to the strong negatively charged characteristics of the SPN-20 separation layer [24,59]. On the other hand, the lowest rejection for $CaCl_2$ was due to the strong affinity of Ca^{2+} cations to the sulfonic acid groups in SPN-20

copolymers. As for NaCl and $MgSO_4$ rejections, the rejection values of $MgSO_4$ exceeded those of NaCl from the point of T_d = 175 °C. This was because the narrower pore size of SPN-20 layers formed under higher drying temperatures led to a pronounced sieving effect for larger $MgSO_4$ ions (M_w = 120.37) compared with that of NaCl (M_w = 58.44).

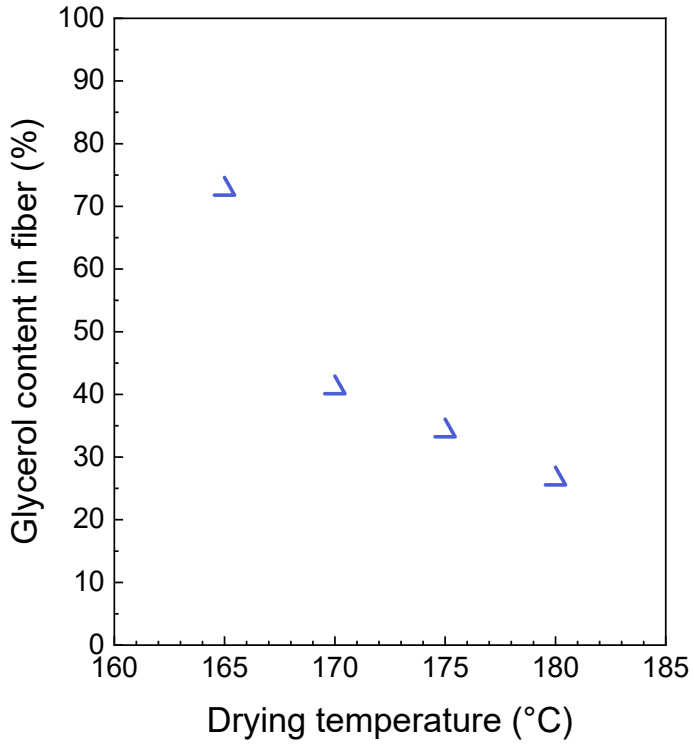

Fig. 10. The glycerol content dependency on drying temperature retained in fiber samples following the dip-coating and drying processes. Before dip-coating, the initial glycerol (and water) content was 350 wt%.

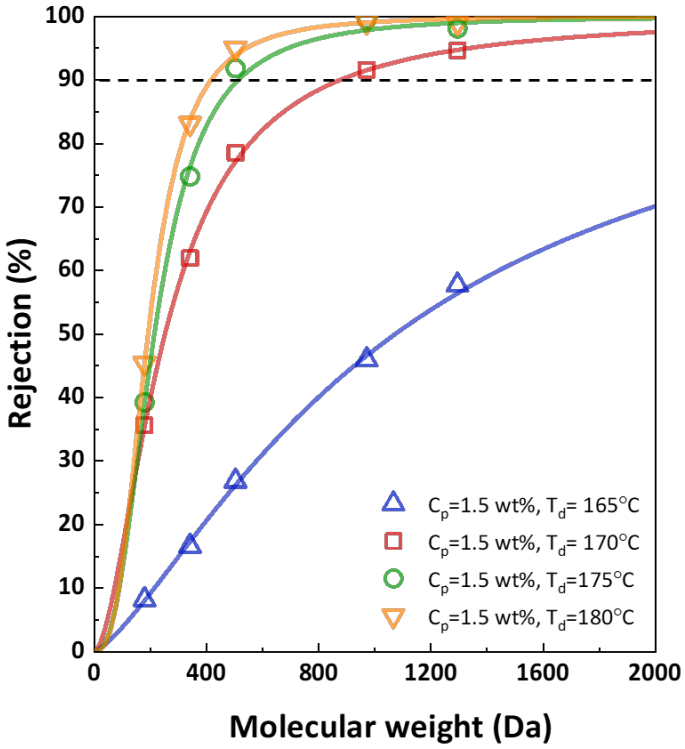

Fig. 11. The MWCO dependency on drying temperature for C_p = 1.5 wt% using five sugars as neutral solutes: glucose (M_w =180.2), sucrose (M_w =342.3), raffinose (M_w =504.4), α-cyclodextrin (M_w =972.8), and γ-cyclodextrin (M_w =1297.1). The feed solute concentrations were 200 mg/L, and the operating pressure was 5 bar. The MWCO values determined at R_j = 90% were estimated to be 890, 520, 420, for T_d = 170, 175, 180 °C, respectively.

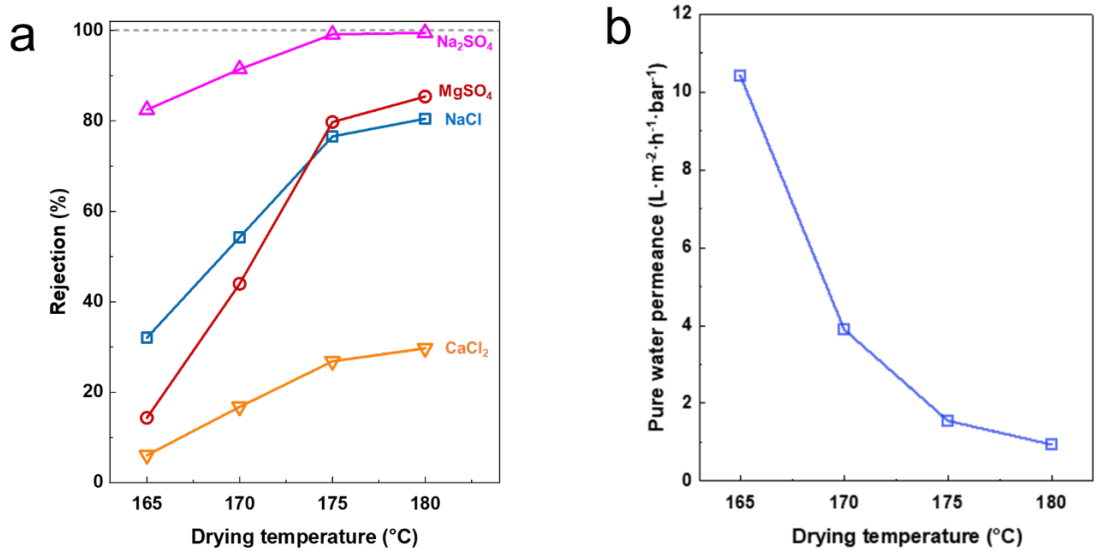

Fig. 12. Dependencies of (a) several salt rejections and (b) pure water permeance of TFC-HF membranes prepared at C_p = 1.5 wt% on drying temperature. Feed salt concentrations were 1,500 mg/L, and the operating pressure was 5 bar.

Table 3. Rejections of negatively charged dyes of the TFC-HF membranes prepared at C_p = 1.5 wt%. The rejection value of 100% represents the point at which the absorbance in the permeate fell below the detection limits (at least R_{ej} > 99.9%).

Membrane	Drying temperature, T_d (°C)	R_{ej} of Evans Blue (M.W. = 960.79) (%)	R_{ej} of Sunset Yellow (M.W. = 452.36) (%)
TFC-HF	165	100	88.6
	170	100	99.7
	175	100	100
	180	100	100

Table. 3 shows the Dependencies of the rejection performances of the TFC-HF membranes for negatively charged organic dyes on drying temperature. The TFC-HF membranes showed almost perfect rejections of Evans Blue even for the loosest membrane prepared at T_d = 165 °C. On the other hand, smaller Sunset Yellow molecules somewhat passed through the separation layer prepared at T_d = 165 and 170 °C. The pure water permeance of the TFC-HF membranes (Fig. 12b) varied from 1.0 to 10.3 ($L \cdot m^{-2} \cdot h^{-1} \cdot bar^{-1}$) depending on the drying temperatures from T_d = 165 to 180 °C. Regarding the stability of these membrane performances, we observed no clear change in flux and separation properties of the TFC-HF membranes after the continuous crossflow NF operation at 5 bar using 1500 ppm-NaCl solution for at least 24 hours. In addition, we found that a backwash treatment using pure water at 5 bar for 30 min also made no change in the membrane performances. Therefore, a durability of the SPN-20 separation layer is fairy excellent.

The membrane performance prepared at T_d = 170 °C (the pure water permeance of 3.9 [$L \cdot m^{-2} \cdot h^{-1} \cdot bar^{-1}$] and MWCO = 890) could be comparable to a commercially available flat-sheet type of the TFC membrane derived from a sulfonated polyethersulfone (SPES) whose pure water permeance was reported to be 12 ($L \cdot m^{-2} \cdot h^{-1} \cdot bar^{-1}$) with the MWCO value between 600 and 800 [60,61]. Despite the permeance value of the TFC-HF membrane prepared at T_d = 170 °C is about three times lower than that of the commercial flat-sheet membrane, these results are promising considering the significant advantage of the higher surface area of hollow-fiber membrane configurations, which could be 7 to 10 times larger per unit volume compared with spiral-wound types of membrane modules.

4. Conclusions

In this study, we demonstrated that PPO hollow-fiber membranes were suitable substrates for TFC-HF membrane fabrication by utilizing a disulfonated poly(arylene ether sulfone) copolymer (SPN-20) that showed a very narrow solubility window. DMSO proved to be a promising solvent that completely dissolved SPN-20 but had no adverse effects on PPO membranes. Fundamental analysis was performed on the dip-coating process, and the thickness and separation of the TFC-HF layer was systematically optimized. The resultant TFC-HF membrane showed excellent nanofiltration performance and reasonable levels of pure water flux.

5. Acknowledgement

The authors gratefully thank members of the Toyobo Analysis Center; Ms. Miyuki Yao provided the SEM and TEM measurements, and Mr. Kazuyuki Oya performed the AFM and XPS measurements.

Author statement

Takashi Ohkame: Conceptualization, Methodology, Validation, Formal analysis, Investigation, Data curation, Writing - original draft, Writing - review & editing.

Masafumi Shibuya: Validation, Investigation.

Keizo Nakagawa: Conceptualization, Methodology, Writing - review & editing.

Takuji Shintani: Conceptualization, Methodology, Writing - review & editing.

Hideto Matsuyama: Conceptualization.

Tomohisa Yoshioka: Conceptualization, Methodology, Writing - review & editing, Supervision.

Declaration of competing interest

The authors declare no conflict of interest.

References

[1] W.J. Koros, Y.H. Ma, T. Shimidzu, Terminology for membranes and membrane processes (IUPAC Recommendations 1996), Pure Appl. Chem. 68 (1996) 1479–1489. https://doi.org/10.1351/pac199668071479.

[2] Y. Yoon, G. Amy, J. Cho, N. Her, Effects of retained natural organic matter (NOM) on NOM rejection and membrane flux decline with nanofiltration and ultrafiltration, Desalination. 173 (2005) 209–221. https://doi.org/10.1016/j.desal.2004.06.213.

[3] Á. de la Rubia, M. Rodríguez, V.M. León, D. Prats, Removal of natural organic matter and THM formation potential by ultra- and nanofiltration of surface water, Water Res. 42 (2008) 714–722. https://doi.org/10.1016/j.watres.2007.07.049.

[4] Figoli, I. Fuoco, C. Apollaro, M. Chabane, R. Mancuso, B. Gabriele, R. De Rosa, G. Vespasiano, D. Barca, A. Criscuoli, Arsenic-contaminated groundwaters remediation by nanofiltration, Sep. Purif. Technol. 238 (2020). https://doi.org/10.1016/j.seppur.2019.116461.

[5] R.S. Harisha, K.M. Hosamani, R.S. Keri, S.K. Nataraj, T.M. Aminabhavi, Arsenic removal from drinking water using thin film composite nanofiltration membrane, Desalination. 252 (2010) 75–80. https://doi.org/10.1016/j.desal.2009.10.022.

[6] A. Caus, S. Vanderhaegen, L. Braeken, B. Van der Bruggen, Integrated nanofiltration cascades with low salt rejection for complete removal of pesticides in drinking water

production, Desalination. 241 (2009) 111–117. https://doi.org/10.1016/j.desal.2008.01.061.

[7] B. Van Der Bruggen, B. Daems, D. Wilms, C. Vandecasteele, Mechanisms of retention and flux decline for the nanofiltration of dye baths from the textile industry, Sep. Purif. Technol. 22 (2001) 519–528. https://doi.org/10.1016/S1383-5866(00)00134-9.

[8] X.L. Wang, T. Tsuru, S.I. Nakao, S. Kimura, The electrostatic and steric-hindrance model for the transport of charged solutes through nanofiltration membranes, J. Membr. Sci. 135 (1997) 19–32. https://doi.org/10.1016/S0376-7388(97)00125-7.

[9] X.L. Wang, Y.Y. Fang, C.H. Tu, B. van der Bruggen, Modelling of the separation performance and electrokinetic properties of nanofiltration membranes, Int. Rev. Phys. Chem. 31 (2012) 111–130. https://doi.org/10.1080/0144235X.2012.659049.

[10] V. Freger, Nanoscale Heterogeneity of Polyamide Membranes Formed by Interfacial Polymerization, Langmuir. 19 (2003) 4791–4797. https://doi.org/10.1021/la020920q.

[11] O. Coronell, B.J. Mariñas, D.G. Cahill, Depth Heterogeneity of Fully Aromatic Polyamide Active Layers in Reverse Osmosis and Nanofiltration Membranes, Environ. Sci. Technol. 45 (2011) 4513–4520. https://doi.org/10.1021/es200007h.

[12] A. Tiraferri, M. Elimelech, Direct quantification of negatively charged functional groups on membrane surfaces, J. Membr. Sci. 389 (2012) 499–508. https://doi.org/10.1016/j.memsci.2011.11.018.

[13] D.L. Shaffer, M.E. Tousley, M. Elimelech, Influence of polyamide membrane surface chemistry on gypsum scaling behavior, J. Membr. Sci. 525 (2017) 249–256. https://doi.org/10.1016/j.memsci.2016.11.003.

[14] G.M. Geise, H.-S. Lee, D.J. Miller, B.D. Freeman, J.E. McGrath, D.R. Paul, Water purification by membranes: The role of polymer science, J. Polym. Sci. Part B Polym. Phys. 48 (2010) 1685–1718. https://doi.org/10.1002/polb.22037.

[15] G. Chowdhury, B. Kruczek, T. Matsuura, eds., Polyphenylene Oxide and Modified Polyphenylene Oxide Membranes, Springer US, Boston, MA, 2001. https://doi.org/10.1007/978-1-4615-1483-1.

[16] M.A. Hickner, H. Ghassemi, Y.S. Kim, B.R. Einsla, J.E. McGrath, Alternative polymer systems for proton exchange membranes (PEMs), Chem. Rev. 104 (2004) 4587–4611. https://doi.org/10.1021/cr020711a.

[17] S. Yang, C. Gong, R. Guan, H. Zou, H. Dai, Sulfonated poly(phenylene oxide) membranes as promising materials for new proton exchange membranes, Polym. Adv. Technol. 17 (2006) 360–365. https://doi.org/10.1002/pat.718.

[18] J.F. Blanco, Q.T. Nguyen, P. Schaetzel, Sulfonation of polysulfones: Suitability of the sulfonated materials for asymmetric membrane preparation, J. Appl. Polym. Sci. 84 (2002) 2461–2473. https://doi.org/10.1002/app.10536.

[19] B. Baradie, C. Poinsignon, J.. Sanchez, Y. Piffard, G. Vitter, N. Bestaoui, D. Foscallo, A. Denoyelle, D. Delabouglise, M. Vaujany, Thermostable ionomeric filled membrane for H2/O2 fuel cell, J. Power Sources. 74 (1998) 8–16. https://doi.org/10.1016/S0378-7753(97)02816-4.

[20] Y. Devrim, S. Erkan, N. Baç, I. Eroğlu, Preparation and characterization of sulfonated polysulfone/titanium dioxide composite membranes for proton exchange membrane fuel cells, Int. J. Hydrogen Energy. 34 (2009) 3467–3475. https://doi.org/10.1016/j.ijhydene.2009.02.019.

[21] D. Lu, H. Zou, R. Guan, H. Dai, L. Lu, Sulfonation of polyethersulfone by chlorosulfonic acid, Polym. Bull. 54 (2005) 21–28. https://doi.org/10.1007/s00289-005-0361-x.

[22] R. Guan, H. Zou, D. Lu, C. Gong, Y. Liu, Polyethersulfone sulfonated by chlorosulfonic acid and its membrane characteristics, Eur. Polym. J. 41 (2005) 1554–1560. https://doi.org/10.1016/j.eurpolymj.2005.01.018.

[23] M. Dalwani, G. Bargeman, S.S. Hosseiny, M. Boerrigter, M. Wessling, N.E. Benes, Sulfonated poly(ether ether ketone) based composite membranes for nanofiltration of acidic and alkaline media, J. Membr. Sci. 381 (2011) 81–89. https://doi.org/10.1016/j.memsci.2011.07.018.

[24] T. He, M. Frank, M.H.V. Mulder, M. Wessling, Preparation and characterization of nanofiltration membranes by coating polyethersulfone hollow fibers with sulfonated poly(ether ether ketone) (SPEEK), J. Membr. Sci. 307 (2008) 62–72. https://doi.org/10.1016/j.memsci.2007.09.016.

[25] H.B. Park, B.D. Freeman, Z.-B. Zhang, M. Sankir, J.E. McGrath, Highly Chlorine-Tolerant Polymers for Desalination, Angew. Chemie. 120 (2008) 6108–6113. https://doi.org/10.1002/ange.200800454.

[26] C.H. Lee, B.D. McCloskey, J. Cook, O. Lane, W. Xie, B.D. Freeman, Y.M. Lee, J.E. McGrath, Disulfonated poly(arylene ether sulfone) random copolymer thin film composite membrane fabricated using a benign solvent for reverse osmosis applications, J. Membr. Sci. 389 (2012) 363–371. https://doi.org/10.1016/j.memsci.2011.11.001.

[27] Y. Sakaguchi, K. Kitamura, S. Nagahara, S. Takase, Preparation of sulfonated poly(ether sulfone nitrile)s and characterization as proton conducting membranes ,Polym. Prepr. 45 (2004), 56.

[28] M.J. Sumner, W.L. Harrison, R.M. Weyers, Y.S. Kim, J.E. McGrath, J.S. Riffle, A. Brink, M.H. Brink, Novel proton conducting sulfonated poly(arylene ether) copolymers containing aromatic nitriles, J. Membr. Sci. 239 (2004) 199–211. https://doi.org/10.1016/j.memsci.2004.03.031.

[29] Y. Gao, G.P. Robertson, M.D. Guiver, S.D. Mikhailenko, X. Li, S. Kaliaguine, Synthesis of Copoly(aryl ether ether nitrile)s Containing Sulfonic Acid Groups for PEM Application, Macromolecules. 38 (2005) 3237–3245. https://doi.org/10.1021/ma047572e.

[30] F. Wang, M. Hickner, Y.S. Kim, T.A. Zawodzinski, J.E. McGrath, Direct polymerization of sulfonated poly(arylene ether sulfone) random (statistical) copolymers: candidates for new proton exchange membranes, J. Membr. Sci. 197 (2002) 231–242. https://doi.org/10.1016/S0376-7388(01)00620-2.

[31] W.W.Y. Lau, M.D. Guiver, T. Matsuura, Phase separation in polysulfone/solvent/water and polyethersulfone/solvent/water systems, J. Membr. Sci. 59 (1991) 219–227. https://doi.org/10.1016/S0376-7388(00)81185-0.

[32] I.M.A. ElSherbiny, R. Ghannam, A.S.G. Khalil, M. Ulbricht, Isotropic macroporous polyethersulfone membranes as competitive supports for high performance polyamide desalination membranes, J. Membr. Sci. 493 (2015) 782–793. https://doi.org/10.1016/j.memsci.2015.05.064.

[33] A. Rahimpour, M. Jahanshahi, N. Mortazavian, S.S. Madaeni, Y. Mansourpanah, Preparation and characterization of asymmetric polyethersulfone and thin-film composite polyamide nanofiltration membranes for water softening, Appl. Surf. Sci. 256 (2010) 1657–1663. https://doi.org/10.1016/j.apsusc.2009.09.089.

[34] A. Idris, N. Mat Zain, M.Y. Noordin, Synthesis, characterization and performance of asymmetric polyethersulfone (PES) ultrafiltration membranes with polyethylene glycol of different molecular weights as additives, Desalination. 207 (2007) 324–339. https://doi.org/10.1016/j.desal.2006.08.008.

[35] M.T. Tsehaye, J. Wang, J. Zhu, S. Velizarov, B. Van der Bruggen, Development and characterization of polyethersulfone-based nanofiltration membrane with stability to hydrogen peroxide, J. Membr. Sci. 550 (2018) 462–469. https://doi.org/10.1016/j.memsci.2018.01.022.

[36] T. Marino, F. Galiano, S. Simone, A. Figoli, DMSO EVOL^{TM} as novel non-toxic solvent for polyethersulfone membrane preparation, Environ. Sci. Pollut. Res. 26 (2019) 14774–14785. https://doi.org/10.1007/s11356-018-3575-9.

[37] D. Hou, H. Fan, Q. Jiang, J. Wang, X. Zhang, Preparation and characterization of PVDF flat-sheet membranes for direct contact membrane distillation, Sep. Purif. Technol. 135 (2014) 211–222. https://doi.org/10.1016/j.seppur.2014.08.023.

[38] K. Khulbe, The morphology characterisation and performance of dense PPO membranes for gas separation, J. Membr. Sci. 135 (1997) 211–223. https://doi.org/10.1016/S0376-7388(97)00138-5.

[39] F. Hamad, T. Matsuura, Performance of gas separation membranes made from sulfonated brominated high molecular weight poly(2,4-dimethyl-l,6-phenyIene oxide), J. Membr. Sci. 253 (2005) 183–189. https://doi.org/10.1016/j.memsci.2004.11.036.

[40] M. Yoshimune, I. Fujiwara, H. Suda, K. Haraya, Novel Carbon Molecular Sieve Membranes Derived from Poly(phenylene oxide) and Its Derivatives for Gas Separation, Chem. Lett. 34 (2005) 958–959. https://doi.org/10.1246/cl.2005.958.

[41] M. Khayet, J.P.G. Villaluenga, M.P. Godino, J.I. Mengual, B. Seoane, K.C. Khulbe, T. Matsuura, Preparation and application of dense poly(phenylene oxide) membranes in pervaporation, J. Colloid Interface Sci. 278 (2004) 410–422. https://doi.org/10.1016/j.jcis.2004.06.021.

[42] C.-Y. Shih, S.-H. Chen, R.-M. Liou, J.-Y. Lai, J.-S. Chang, Pervaporation separation of water/ethanol mixture by poly(phenylene oxide) and sulfonated poly(phenylene oxide) membranes, J. Appl. Polym. Sci. 105 (2007) 1566–1574. https://doi.org/10.1002/app.25365.

[43] M. Yoshimune, I. Fujiwara, K. Haraya, Carbon molecular sieve membranes derived from trimethylsilyl substituted poly(phenylene oxide) for gas separation, Carbon N. Y. 45 (2007) 553–560. https://doi.org/10.1016/j.carbon.2006.10.017.

[44] D. Li, R. Wang, T.S. Chung, Fabrication of lab-scale hollow fiber membrane modules with high packing density, Sep. Purif. Technol. 40 (2004) 15–30. https://doi.org/10.1016/j.seppur.2003.12.019.

[45] M. Sekino, Study of an analytical model for hollow fiber reverse osmosis module systems, Desalination. 100 (1995) 85–97. https://doi.org/10.1016/0011-9164(96)00010-0.

[46] C.M. Hansen, Hansen Solubility Parameters, CRC Press, 2007. https://doi.org/10.1201/9781420006834.

[47] H.M. Colquhoun, D. Chappell, A.L. Lewis, D.F. Lewis, G.T. Finlan, P.J. Williams, Chlorine tolerant, multilayer reverse-osmosis membranes with high permeate flux and high salt rejection, J. Mater. Chem. 20 (2010) 4629. https://doi.org/10.1039/b926352g.

[48] D.A. White, J.A. Tallmadge, A theory of withdrawal of cylinders from liquid baths, AIChE J. 12 (1966) 333–339. https://doi.org/10.1002/aic.690120223.

[49] D. Quéré, FLUID COATING ON A FIBER, Annu. Rev. Fluid Mech. 31 (1999) 347–384. https://doi.org/10.1146/annurev.fluid.31.1.347.

[50] P. Długołecki, K. Nymeijer, S. Metz, M. Wessling, Current status of ion exchange membranes for power generation from salinity gradients, J. Membr. Sci. 319 (2008) 214–222. https://doi.org/10.1016/j.memsci.2008.03.037.

[51] M. DuBois, K.A. Gilles, J.K. Hamilton, P.A. Rebers, F. Smith, Colorimetric Method for Determination of Sugars and Related Substances, Anal. Chem. 28 (1956) 350–356. https://doi.org/10.1021/ac60111a017.

[52] N.A. Ochoa, P. Prádanos, L. Palacio, C. Pagliero, J. Marchese, A. Hernández, Pore size distributions based on AFM imaging and retention of multidisperse polymer solutes: Characterisation of polyethersulfone UF membranes with dopes containing different PVP, J. Membr. Sci. 187 (2001) 227–237. https://doi.org/10.1016/S0376-7388(01)00348-9.

[53] J. P. Teas, Graphic analysis of resin solubilities, J. Paint Technol. 40 (1968) 19–25.

[54] S. Mahalingam, B.T. Raimi-Abraham, D.Q.M. Craig, M. Edirisinghe, Solubility-spinnability map and model for the preparation of fibres of polyethylene (terephthalate)

using gyration and pressure, Chem. Eng. J. 280 (2015) 344–353. https://doi.org/10.1016/j.cej.2015.05.114.

[55] T. Marino, F. Russo, A. Figoli, The formation of polyvinylidene fluoride membranes with tailored properties via vapour/non-solvent induced phase separation, Membranes (Basel). 8 (2018) 1–17. https://doi.org/10.3390/membranes8030071.

[56] M. Weng, Determination of the Hansen solubility parameters with a novel optimization method, J. Appl. Polym. Sci. 133 (2016) 1–6. https://doi.org/10.1002/app.43328.

[57] N. Mys, R. Van De Sande, A. Verberckmoes, L. Cardon, Processing of polysulfone to free flowing powder by mechanical milling and spray drying techniques for use in selective laser sintering, Polymers (Basel). 8 (2016). https://doi.org/10.3390/polym8040150.

[58] H.J. Oh, B.D. Freeman, J.E. McGrath, C.H. Lee, D.R. Paul, Thermal analysis of disulfonated poly(arylene ether sulfone) plasticized with poly(ethylene glycol) for membrane formation, Polymer, 55, (2014) 235–247. https://doi.org/10.1016/j.polymer.2013.11.041.

[59] T. Tsuru, M. Urairi, S. ichi Nakao, S. Kimura, Reverse osmosis of single and mixed electrolytes with charged membranes: Experiment and analysis, J. Chem. Eng. Japan. 24 (1991) 518–524. https://doi.org/10.1252/jcej.24.518.

[60] B. Van der Bruggen, J. Schaep, W. Maes, D. Wilms, C. Vandecasteele, Nanofiltration as a treatment method for the removal of pesticides from ground waters, Desalination. 117 (1998) 139–147. https://doi.org/10.1016/S0011-9164(98)00081-2.

[61] B. Mi, O. Coronell, B.J. Mariñas, F. Watanabe, D.G. Cahill, I. Petrov, Physico-chemical characterization of NF/RO membrane active layers by Rutherford backscattering

spectrometry, J. Membr. Sci. 282 (2006) 71–81. https://doi.org/10.1016/j.memsci.2006.05.015.